Nanoscale

Dynamic Article Links

Cite this: *Nanoscale*, 2012, **4**, 4883

www.rsc.org/nanoscale

FEATURE ARTICLE

Patterning of graphene

Ji Feng,[a] Wenbin Li,[b] Xiaofeng Qian,[b] Jingshan Qi,[c] Liang Qi[b] and Ju Li*[b]

Received 2nd April 2012, Accepted 4th June 2012
DOI: 10.1039/c2nr30790a

Two-dimensional atomic sheets of carbon (graphene, graphane, *etc.*) are amenable to unique patterning schemes such as cutting, bending, folding and fusion that are predicted to lead to interesting properties. In this review, we present theoretical understanding and processing routes for patterning graphene and highlight potential applications. With more precise and scalable patterning, the prospects of integrating flat carbon (graphene) with curved carbon (nanotubes and half nanotubes) and programmable graphene folding are envisioned.

1. Introduction

Since the isolation by Andre Geim and Kostya Novoselov of the first free-standing, atomically thin membrane, graphene in 2005,[1] the field has attracted tremendous attention. This serendipitous finding was seemingly simple, involving exfoliating monolayers of graphite by writing with a pencil on a scotch tape. But the ensuing impact on physics, materials science and chemistry has been broad, entailing many fundamental findings and ingenuous discoveries. The interest in graphene owes its origin largely to its electronic structure. As a two-dimensional (2D) material, the electronic states of graphene depart dramatically from the conventional 2D semiconductor epitaxial layers. The low-energy excitation spectrum in graphene mimics that of massless Dirac fermions, with a "modest" Fermi velocity of $\sim 10^6$ m s^{-1} which is independent of its momentum, favouring ballistic quantum transport with high electron mobility and long phase coherent length.[2] All these relativistic-like behaviours arise not from all the reasoning behind the Dirac equations, but from the geometrically simple, yet aesthetically intriguing, bipartite honeycomb lattice. When a perpendicular external magnetic field is applied, the electrons in graphene, which are constrained to move in the plane of the honeycomb lattice, circulate in closed loop orbits under the Lorentz force. The cyclotron orbits in the $\boldsymbol{k}$-space are quantized, leading to the unconventional quantum Hall states.

[a]*International Center for Quantum Materials, School of Physics, Peking University, Beijing 100871, China*
[b]*Department of Nuclear Science and Engineering and Department of Materials Science and Engineering, Massachusetts Institute of Technology, Cambridge, Massachusetts 02139, USA. E-mail: liju@mit.edu*
[c]*College of Physics and Electronic Engineering, Jiangsu Normal University, Xuzhou 221116, China*

Ji Feng

Ji Feng is an associate professor of physics, in the International Center for Quantum Materials at Peking University, China. Combining quantum theory and ab initio *simulation, his research group (www.phy.pku.edu.cn/~jfeng/) studies chemical, mechanical, magnetic and optical properties of novel quantum materials. Ji Feng obtained his Ph.D. degree in chemistry at Cornell University in 2007. He worked with Professor Ju Li as a post-doctoral researcher between 2009 and 2011. He was awarded the Wentink Prize (Cornell University, 2007) for his thesis work, and the 1000 Young Investigator Award of China in 2011.*

Wenbin Li

Wenbin Li is a graduate student in the Department of Materials Science and Engineering at MIT, under the supervision of Professor Ju Li. He studies electrical, chemical and mechanical properties of nanomaterials such as graphene and colloidal nanoparticles using ab initio *and molecular dynamics simulation. He obtained a Bachelor's degree from Zhejiang University in China and a Master's degree from University of Pennsylvania, both in Materials Science and Engineering.*

A quick glimpse of the physics of graphene immediately invites thoughts about its application – from "what it is" to "what it can be". In order to bring the immense potential of graphene into the solution to such technological challenges as nanoscopic electronics and energy storage, there is plenty of room to explore given the rich physics. But taking a historical perspective from the evolution of the silicon technology, we see that it is not just the intrinsic semiconducting properties that drive the progress of this society-transforming industry; it is rather how we can control its properties and shape. The key momentum is in fact provided by the ability to precisely tune the conductivity through controlled doping and to fabricate high quality complex patterns on a silicon surface at affordable cost. Naturally, the ability to do the same for graphene-based materials will be highly desired. What also necessitates the need for patterning graphene is the fact that flat and wide graphene is intrinsically a semimetal, which makes it difficult to envision direct application in semiconductor devices. First-principles calculations and experimental measurements suggest that the direct band gap of graphene nanoribbons scales inversely with their widths.[3–5] Patterning graphene into finite structures with nanometer-scale confinement is thus also important for tuning the transport properties of graphene-based devices. It is essential for us to learn how to create patterned structures with graphene, and in doing so, to control the properties of graphene.

Now imagine we are tailors and are asked what we can make from a cloth. We can surely cut it, fold it, crease it and sew on it. We naturally would like to do the same on graphene: cleaving

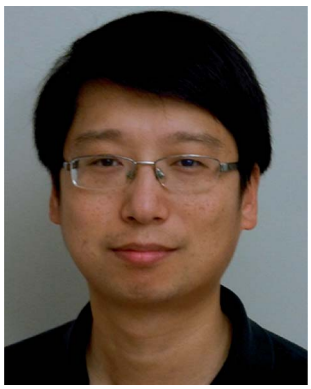

Xiaofeng Qian

Xiaofeng Qian is a postdoctoral associate in Professor Ju Li's group. He works on the development of first-principles methods based on density functional theory and many-body perturbation theory to investigate ground-state and excited-state properties of nanostructured materials and design functional electronic, spintronic, and photovoltaic devices. He obtained his Ph.D. degree in Nuclear Science and Engineering from MIT in 2008, and Bachelor's degree in Engineering Physics from Tsinghua University in China in 2001. He and Professor Ju Li have developed ab initio *quasi-atomic orbitals and time-dependent density functional theory with ultrasoft pseudopotentials.*

Liang Qi

Liang Qi is a postdoctoral associate in Professor Ju Li's group. He works on first-principles and atomistic modeling of materials for energy storagel conversion (catalysts of fuel cells, lithium-ion battery electrodes) and nanostructured materials with special electronic and mechanical properties. He obtained his Ph.D. degree in Materials Science at University of Pennsylvania in 2009, Master's degree in Materials Science at the Ohio State University in 2007 and Bachelor's degree in Materials Science and Engineering at Tsinghua University in China in 2003.

Jingshan Qi

Jingshan Qi is an Assistant Professor in the College of Physics and Electronic Engineering, Jiangsu Normal University, China. He investigates mechanical, electronic and transport properties of materials by atomistic modelling, first-principles electronic structure calculations and theoretical models. Recently his research interests focus on one-dimensional nanostructures, two-dimensional atomic membranes and elastic-strain-engineering of nanomaterials. Jingshan obtained a Ph.D. degree in Condensed Matter Physics from Nanjing University of Aeronautics and Astronautics in 2011. From 2009 to 2010, he was studying in Professor Ju Li's Group.

Ju Li

Ju Li is Battelle Energy Alliance Professor of Nuclear Science and Engineering and a Full Professor of Materials Science and Engineering at MIT. Using atomistic modelling and in situ *experiments, his group (http://li.mit.edu) investigates mechanical, electrochemical and transport behaviours of materials, often under extreme stress, temperature and radiation environments. Ju obtained a Ph.D. degree in nuclear engineering from MIT in 2000, and Bachelor's degree in Physics from University of Science and Technology of China in 1994. He is a winner of the 2005 Presidential Early Career Award for Scientists and Engineers, 2006 MRS Outstanding Young Investigator Award, and 2007 TR35 award from the* Technology Review *magazine.*

chemical bonds, chemical modification of the bonding pattern, and creating wrinkles on graphene. In Table 1 we summarize the energy scales and/or essential material properties pertinent to these fundamental processes. It is clear that there is an energetic hierarchy in various processes involved in tailoring graphene. The most radical approach is selectively breaking C–C bonds, which can be achieved by irradiation with energetic electrons[6,7] or chemical reactions, or high temperature treatment.[8] On the lower end of the energy hierarchy, one finds energetically cheap elastic bending, whence the rich physics of elastic membrane[9,10] can be explored at the thinnest limit. Physisorption and chemisorption are also possible pathways for creating patterns on graphene. Both elastic and adsorptive processes have the advantage of reversibility.

To this end, this review will recapitulate recent progress in creating patterns on graphene, and we hope to propose a couple of strategies in this direction. The selection of topics and materials here is by no means exhaustive. For general reviews on graphene, we refer the readers to other literature[24–27] and also instructive reviews;[28,29] there are also reviews for the electronic structure of graphene[30] and preparation techniques.[31,32]

2. Direct bond cleavage and formation

It has been envisioned that nanostructures and devices may be fabricated by directly carving mono- or multilayer graphene, very early in "the rise of graphene",[24] and actually, long before that (see Fig. 1a).[33] Mechanical cutting has recently been applied. The energy it takes to rip off an atom from a graphene lattice is estimated to be ~17 eV,[11] implying that the energy for cleaving a single carbon bond is ~5 to 6 eV. In order to create patterns on graphene by cleavage of C–C bonds, energetic carving tools are needed. These include direct mechanical cleavage,[24,33] electron beam irradiation,[8,11,34–39] scanning probe lithography,[40–42] helium ion beam lithography,[43,44] photocatalytic etching,[45] plasma etching,[46–50] chemical etching,[4,51–57] and nanoimprint lithography.[58] Alternatively, bottom-up synthetis[59–65] and reduction of graphene oxide[66–71] can form patterned structures directly, without breaking pre-existent carbon–carbon bonds.

Since transmission electron microscopy (TEM) is a standard tool to observe atomic structure and nanoscale morphology, high-energy (80–300 keV) electron-beam irradiation is often used to fabricate graphene nanostructures. Meyer *et al.*[36] demonstrated that a focused electron beam in TEM can induce deposition of carbon on freestanding graphene membranes to produce nanoscale patterns with the help of periodic grating.

Table 1 Structural energy hierarchy of graphene

Material property	Rough range/scale	Source
Cohesive energy	~−5 to −6 eV per atom	11, 12[a], 13[c]
Interlayer cohesion	~−0.04 eV per atom	14[a], 15[c], 16[b]
Physisorption	H_2:−0.07 to −0.09 eV per H_2	17[b]
Hydrogenation	−0.15 eV per atom	18, 19[b]
Young's modulus, Y	1000 GPa	20[b], 21[a]
Bending modulus, D	0.1–0.4 nN nm	22[a], 23[c]

[a] Experimental value. [b] First-principles calculation. [c] Empirical potential.

Fischbein and Drndić[35] then showed that nanosculpting of suspended graphene sheets by a focused electron beam can make a variety of structures, including nanoscale pores, slits, and gaps. However, because of its high energy, an electron beam often generates unwanted defects, such as amorphization and undesired carbon deposition. These damages can be controlled by reducing the electron energy to 80 keV,[11] but a low-energy beam cannot produce nanoscale patterns efficiently. To solve this problem, Song *et al.*[37] introduced a method of electron-beam nanosculpting at temperatures above 600 °C, which makes carbon ad-atoms mobile to continuously repair the radiation damage. This technique can fabricate near-defect-free single-crystalline graphene nanostructures, such as nanoribbons, nanotubes, nanopores, and single carbon chains. Besides varying external conditions like electron energy and temperature, nanostructured patterning by electron-beam irradiation can also be facilitated by intrinsic properties of graphene defects. Huang *et al.*[8] showed that Joule-heating (~2000 °C) aided by electron beam irradiation can produce a fractal-like "coastline" sublimation pattern on suspended few-layer graphene; further TEM and theoretical studies indicate that the fractal character results from reconstructions of monolayer edges (MLE) into bilayer edges, aka "half nanotubes", which will be discussed in detail later. Cui *et al.*[72] used first-principles calculations to discover certain "magic numbers" of total missing carbon atoms for stable vacancies in single-layer graphene, which could guide e-beam fabrication of nanopores on graphene with stable magnetic-semiconducting properties. In summary, although it is difficult to apply e-beam irradiation to fabricate graphene patterns and devices at large scale and affordable cost, it is an ideal technique when combined with *in situ* TEM observation[8] to explore the possible mechanisms of graphene morphology evolution, which may stimulate the invention of new routines for patterning graphene. For example, recently Chuvilin *et al.*[73] observed that the graphene flake stripped from a single-layer graphene edge by electron beam irradiation could automatically transform into fullerene C_{60} molecule, which is quite different from the fullerene formation mechanism based on carbon-cluster coalescence.

Lithographical methods have been developed to create graphene nanostructures with pre-designed patterns. Lithographical methods can be used to create graphene nanoribbons (GNRs), with width down to ~20 nm, with a roughness on the order of a few nanometres.[39,46] The method employs conventional e-beam lithographical negative resist to form a protective pattern on graphene, which is subsequently exposed to plasma oxygen. The unprotected portion of graphene is then chemically removed upon the attack by the reactive plasma and carried into the vapour phase. The pattern on the mask (and the e-beam resist) then is "printed" into graphene.[39,46] Nanoribbons with width down to 20 nm can be fabricated, and it was shown that the resistivity depends sensitively on the width (see Fig. 1b and c). Han *et al.*[46] used this method to tune the band gap of graphene nanoribbons by fabricating them into different widths. It was also suggested that tunnelling current with a scanning probe can be used to fabricate graphene nanodevices.[24,74] And indeed, a scanning tunnelling microscope (STM) probe can be used to cleave C–C bonds in graphene when operated at a bias voltage (>2 V) much higher than that in topographical measurements (typically ~200 mV). When the probe advances on graphene in

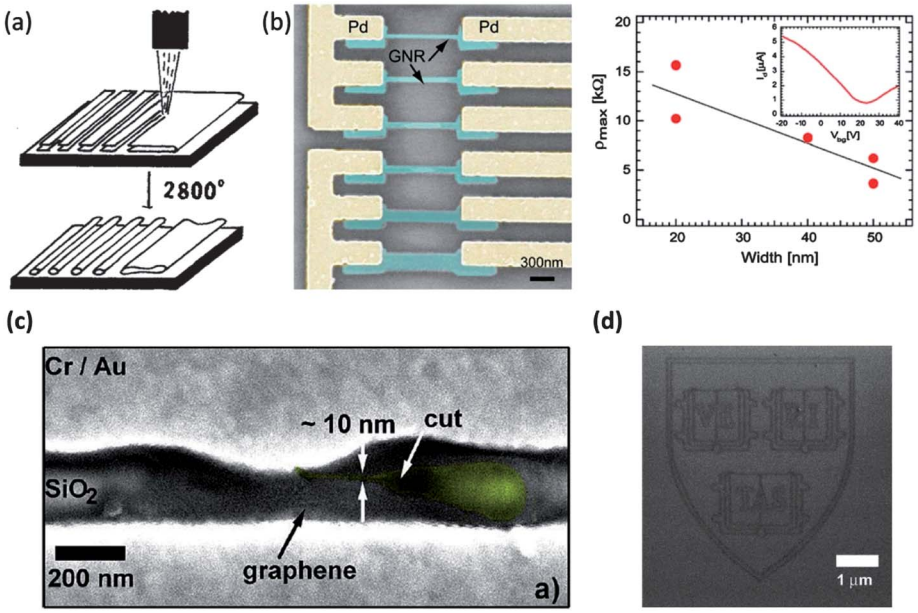

Fig. 1 (a) A visionary insight into graphene carving long before the isolation of graphene.[33] The schematic proposed by Ebbessen and Hiura involves mechanically cutting graphene bilayers with scanning probes, followed by subsequent annealing, to fabricate pre-designed carbon nanostructures. (b) Graphene nanoribbons with controlled widths fabricated by e-beam lithography, and the measured electric resistivity of GNRs as a function of their widths.[39] (c) A suspended graphene device after etching with helium ion lithography. A minimum feature size of about 10 nm can be achieved.[43] (d) The same authors also demonstrated that complex patterns can be created on multi-layer graphene flakes using this technique.[44] (Reprinted with permission from ref. 33, Copyright© 1995 WILEY-VCH; ref. 39, Copyright© 2007 Elsevier; ref. 43, Copyright© 2009 American Chemical Society; ref. 44, Copyright© 2009 IOP Science.)

the carving mode, GNRs as narrow as 10 nm could be produced.[40] These techniques have a high degree of control over the patterns "printed" into graphene, which is quite desirable from a device-fabrication point of view. Naturally, the resolution (feature size and edge roughness) of these methods is limited by instrumentation. The resolution of e-beam lithography depends mainly on the electron beam size and on the scattering and propagation of electrons in the resist material. Line-widths as small as 10 nm can be achieved with modern day field emission electron source and appropriate lensing.[75] As the de Broglie wavelength of helium ion is many times smaller than electron beams for the same acceleration voltage, helium ion beam lithography can give an ultimate resolution of 0.5 nm. This approach was recently demonstrated by Lemme *et al.* to obtain precise cutting and patterning of graphene devices on silicon dioxide substrates with minimum feature size in the 10 nm region (see Fig. 1c and d).[43]

Bai *et al.* developed a way to fabricate graphene nanomeshes with variable periodicities and neck width as low as 5 nm that opens up an electronic transport gap in graphene sheets.[48] A schematic of this process is shown in Fig. 2a. First, a block copolymer thin film with periodic cylindrical domains was formed and annealed on top of a SiO_x-protected graphene flake to develop a porous polymer film. It was then followed by fluoride-based reactive ion etching and oxygen plasma etching process to remove polymer films and silicon oxide, and finally the oxide mask was removed by dipping the sample into HF solution. A similar strategy was utilized by other groups to achieve graphene nanomeshes at different scales.[49,50] Liang *et al.* also fabricated hexagonal graphene nanomeshes with sub-10 nm ribbon width by combining nanoimprint lithography, block copolymer self-assembly, and electrostatic printing.[58] The decrease of ribbon width leads to the increase of the ON/OFF current ratio and thus the bandgap opening, demonstrating its potential application as field-effect transistors (FET).

Datta *et al.*[51] and, later, Ci *et al.*[52] showed that catalytic methanation can be used to carve graphene chemically (the same technique has been used by Tomita and Tamai to carve multilayer graphene or graphite[53]). Metal nanoparticles (Ni[52] or Fe[51]) are first formed on graphene, which upon heating in a hydrogen atmosphere, catalytically etch away the carbon atoms (leaving as gaseous hydrocarbon or CO_2), as shown in Fig. 2b. The metal nanoparticles diffuse along the low-index direction of the graphene lattice as the reaction progresses, to form nanometre-sized trenches (as long as 1 μm). In another work, slender graphene nanoribbons are formed by sonicating graphite dispersed in a 1,2-dichloroethane solution of PmPV (poly(*m*-phenylenevinylene-*co*-2,5-dioctoxy-*p*-phenylenevinylene)).[4] It was suggested that the mechanical energy afforded by sonication and ultrahot gas bubbles is responsible for breaking graphene into fine pieces of slender nanoribbons. Even though the chemistry of this method is not yet well understood, this simple wet chemical approach can produce GNRs with a very high aspect ratio (length/width), with some pieces' widths less than 10 nm with relatively smooth edges (see Fig. 2c). Dimiev *et al.* also developed an etching route for the layer-by-layer removal of graphene.[54] They first sputter-coated zinc on top of multilayer graphene with a predesigned pattern and then removed the zinc and the adjacent single graphene layer in dilute HCl solution. Graphene nanoribbons can also be made from carbon nanotubes from a bond-breaking

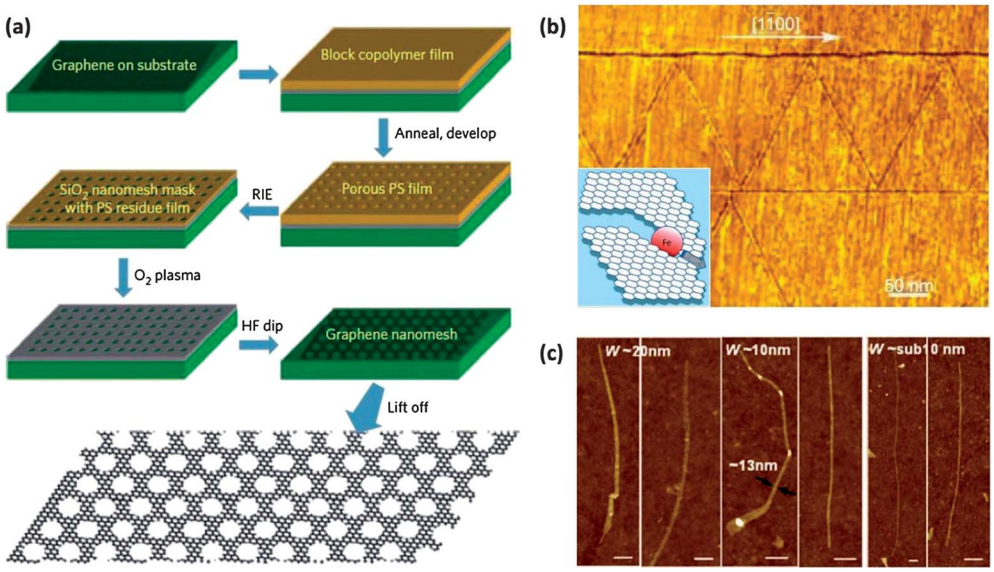

Fig. 2 (a) Schematic of fabricating graphene nanomeshes by block copolymer lithography. A block copolymer thin film with periodic cylindrical domains was first formed and annealed on top of a SiO_x-protected graphene flake to develop a porous polymer film. Fluoride-based reactive ion etching and oxygen plasma etching were then used to punch holes into the graphene layer and remove the polymer film. Finally a graphene nanomesh was obtained by dipping the sample into HF solution to remove the oxide mask.[48] (b) Atomic force micrograph of triangular flakes from cutting graphene by catalytic methanation.[51,52] The scale bar measures 50 nm. Inset: a schematic of the etching process by a migrating catalytic metal nanoparticle. (c) Atomic force micrographs of slender GNRs from a mechanochemical approach.[4] All bars correspond to 100 nm. (Reprinted with permission from ref. 48, Copyright© 2010 Macmillan Publishers Ltd: *Nature Nanotechnology*; ref. 51, Copyright© 2008 American Chemical Society; ref. 52, Copyright© 2008 Springer; ref. 4, Copyright© 2008 AAAS.)

process.[55–57] A carbon nanotube is first cast in a resin, which protects half of the nanotube. Upon exposure to an argon plasma, carbon atoms begin to be removed from one side of the tube. By controlling the time of exposure, nanoribbons with different layers can be prepared upon release from the protective resin.

The key advantage of solution phase chemical etching techniques is the fact that they are comparatively milder than e-beam or scanning probe lithographical methods, and thus can produce smoother edges especially along low-energy directions. However, chemical methods suffer from the lack of architectural control. In the catalytic methanation method, there is almost no control over the final shape of graphene flakes, because the initial distribution of the metal nanoparticles and the dynamics of the nanoparticle diffusion cannot be controlled precisely. An improved version of this technique employs an external magnetic field to guide the diffusion of magnetic catalytic particles, to obtain nanotrenches with pre-designed shapes.[76] Nonetheless, the issue remains with the lack of control over the initial spatial distribution of the nanoparticles before a controlled global patterning can be achieved. For the mechanochemical etching,[4] the ability to control the architecture and dimensions of the nanoribbons is essentially lacking. It might be interesting to develop patterned chemical protection to designated areas on graphene from the mechanochemical attack in order to achieve the desired morphology, which on the other hand requires the knowledge of the actual chemistry of the etching process. In addition, it is important that special techniques must be developed to transfer and deposit these nanoribbons for device applications.

Kim *et al.*[59] demonstrated an elegant approach to grow large scale graphene films on a pre-patterned catalytic surface. A nickel thin film was first grown on a SiO_2 surface, and carbon was deposited on the nickel layer by chemical vapour deposition (CVD) at 1000 °C using $CH_4/H_2/Ar$ as the feedstock. Carbon films spontaneously anneal to few-layer graphene (predominantly bilayers) at room temperature. The process is schematically shown in Fig. 3a. It was also shown that the as-grown graphene layers can be lifted off the nickel substrate with acid etching, and adhere conformally to elastomeric or SiO_2 substrates (see Fig. 3b).

Yang *et al.* developed a novel bottom-up synthetic approach to directly grow GNRs from precursor monomers in solution phase.[60] Recently, Cai *et al.*[61] and Treier *et al.*[62] used an improved synthetic strategy to grow GNRs on metal surfaces with specific patterns, *i.e.*, different topologies and widths at atomic precision (Fig. 3c). This was achieved by first depositing precursor monomers onto clean metal substrates using thermal sublimation. During the same step, dehalogenation and radical addition were also induced, and a linear polymer chain was formed through surface-assisted carbon–carbon coupling. The polymer chain was then annealed at higher temperature, which introduces intramolecular cyclodehydrogenation and leads to hydrogen-terminated fully aromatic GNRs. The pattern of the resultant GNRs was simply controlled by the corresponding precursor monomers. In order to further fabricate devices, special techniques need to be developed to either transfer these nanoribbons onto technologically relevant substrates or directly grow GNRs on the designated substrates. Sprinkle *et al.* demonstrated that it is indeed possible to directly grow patterned graphene on SiC with excellent scalability (Fig. 3d).[63] In addition, self-assembly was adopted to successfully grow graphene on patterned substrates,[64,65] demonstrating itself being another promising route for scalable production.

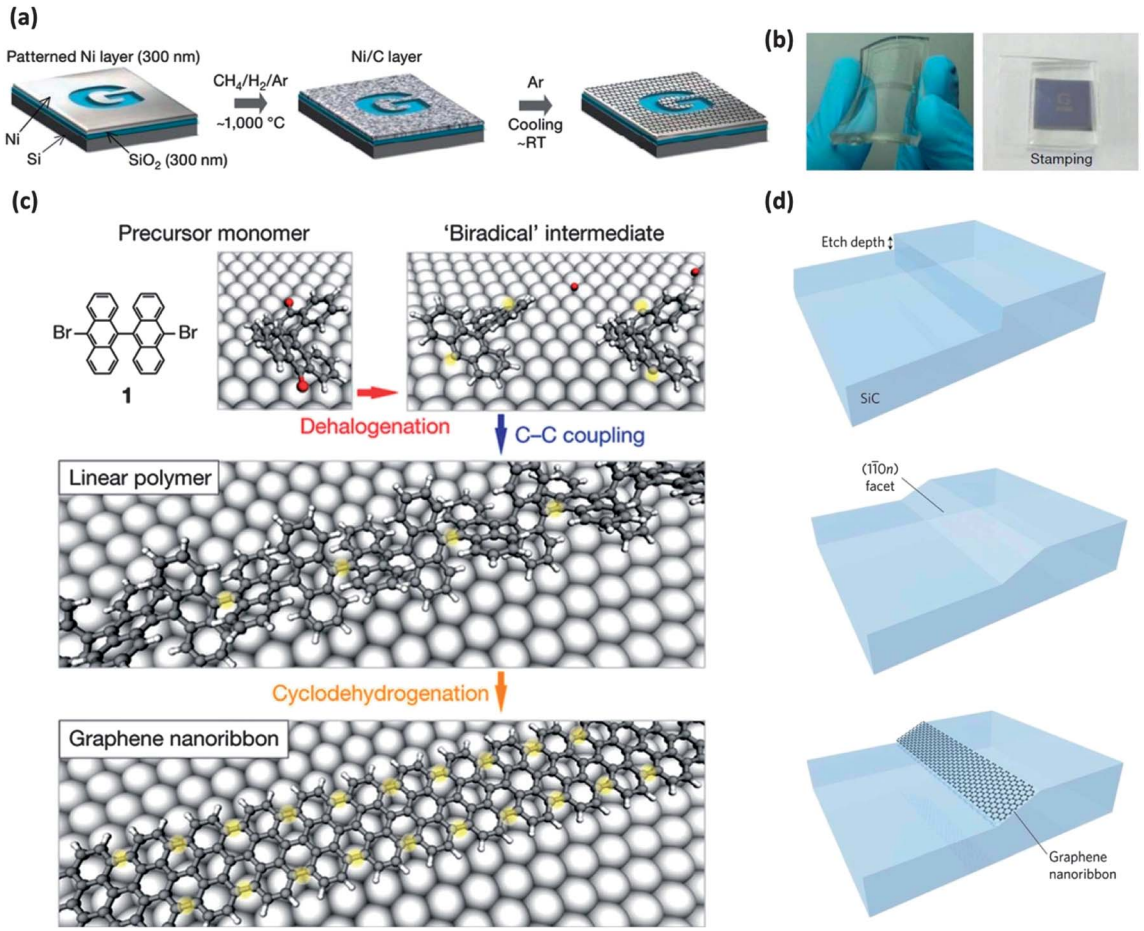

Fig. 3 (a) Schematic of the patterned growth of graphene on a pre-patterned catalytic surface, and (b) the resultant flexible graphene on a transparent elastomeric substrate, and the patterned graphene transferred onto a SiO_2 substrate.[59] (c) Schematic of bottom-up fabrication of atomically precise GNRs. Top, precursor monomers were first deposited onto clean metal substrates using thermal sublimation. Dehalogenation was also induced during this step. Middle, formation of linear polymers by covalent interlinking of the dehalogenated intermediates. Bottom, annealing at higher temperature introduces intramolecular cyclodehydrogenation and leads to hydrogen-terminated fully aromatic GNRs.[61] (d) Self-organized graphene nanoribbon formation on SiC. A nanometre-scale step is etched into the SiC crystal by fluorine-based reactive ion etching. The crystal is then heated to 1200–1300 °C, which induces step flow and relaxation to the (1 $\bar{1}$ 0*n*) facet. Upon further heating to ~1450 °C, self-organized graphene nanoribbon forms on the facet.[63] (Reprinted with permission from ref. 59, Copyright© 2009 Macmillan Publishers Ltd: *Nature*; ref. 61, Copyright© 2010 Macmillan Publishers Ltd: *Nature Nanotechnology*; ref. 63, Copyright© 2010 Macmillan Publishers Ltd: *Nature Nanotechnology*.)

Reduction of graphene oxide through various means such as local thermal reduction,[77,78] photochemical reduction[66] and electrochemical reduction[67] has also been shown to be a viable approach to produce patterned graphene with great tunability. Laser scribing was recently applied by Strong *et al.*,[68] which can directly pattern circuits and complex design in a single step process without masks, templates, and post-processing. It was shown to be an efficient way to deoxygenate the graphite oxide film and produce highly reduced laser scribed graphene with significantly enhanced conductivity with sub-20 nm feature sizes. In addition, the electronic properties of patterned devices can be fine tuned by varying laser intensity and irradiation. As laser scribing can reduce graphite oxide into graphene in a controllable way, El-Kady *et al.* from the same group fabricated a graphene-based electrochemical supercapacitor using a standard LightScribe DVD optical drive, which gives rise to high energy density and fast charge–discharge rate as well as excellent mechanical strength.[69] Zhang *et al.* directly imprinted graphene microcircuits on graphene oxide through direct femtosecond laser reduction with a designed complex pattern in high resolution.[70] The same group demonstrated that the band gap of graphene oxide can be significantly reduced down to the semiconductor regime by tuning the femtosecond laser power.[71]

Finally, a brief summary of different techniques for graphene patterning through direct bond cleavage and formation is given in Table 2.

3. Chemical patterning

Graphene or graphite is chemically very inert, at least at room temperature. For this reason, chemical patterning of graphene has been less explored. Here by "chemical patterning" we refer to the situation involving chemisorption, where the C–C bonds are not cleaved. The underlying σ-bonds are very strong, and it takes much brute force to cleave the graphene membrane. On the other hand, when one considers the delocalized π-bonds, a chemist

Table 2 Summary of different techniques for graphene patterning through direct bond cleavage and formation

Method	Source
Direct mechanical cleavage	24, 33
Electron beam irradiation	8, 11, 34–39
Scanning probe lithography	40–42
Helium ion beam lithography	43
Photocatalytic etching	45
Plasma etching	46–50
Chemical etching	4, 51–57
Nanoimprint lithography	58
Bottom-up growth and synthesis	59–65
Reduction of graphene oxide	66–71

would argue that the inertness of graphene is more of a kinetic issue, drawing analogy from so many addition reactions in organic chemistry that break the pπ bonds while preserving the carbon backbones of organic molecules. The accounting of energy is straightforward: the stability of a π-bond is worth less than a single σ-bond, much less two. For example, addition of a dihydrogen molecule to a double bond is typically exothermic, but is difficult to proceed without appropriate catalysts to help circumvent the kinetic barriers. Graphene is composed of sp^2 bonded carbon atoms, much like a sheet of fused benzene rings. Hydrogenation of benzene to cyclohexane is an exothermic reaction, releasing 210 kJ mol^{-1} of heat ($\Delta H = -0.36$ eV per H atom). It is then no surprise that calculation showed that the energy of formation of graphane, the fully hydrogenated form of graphene, is −0.15 eV per H atom.[19]

Partial hydrogenation of graphene was achieved by decomposing *in situ* a chemical feedstock (*e.g.*, hydrogen silsesquioxane) to generate atomic hydrogen. Elias *et al.* demonstrated that full hydrogenation can be achieved to form graphane, by passing atomic hydrogen over graphene at 300 K.[79] Graphane's structure can be thought of as fused cyclohexane (as graphene is fused benzene; see Fig. 4a), where like in cyclohexane the chair conformation is more stable. Therefore, graphane has the same honeycomb lattice as graphene, only slightly puckered. It might be interesting to note that the symmetry changes on going from graphene to graphane: graphene's principal rotation is pure 6-fold, whereas the principal rotation in fully saturated graphane is 3-fold plus inversion. And the hydrogenation is fully reversible. Upon annealing graphane at 450 K in Ar atmosphere, hydrogen is desorbed and graphene is recovered. As Elias *et al.* showed by measuring the resistivity at different temperatures and with/without external magnetic fields, all the important electronic characteristics of the initiating graphene are recovered (see Fig. 4b).[79,80]

The reversible hydrogenation of graphene opens *gentle* chemical pathways for patterning graphene to tune its properties. One key notion here is that the hydrogenated carbon atom is electronically removed from the sp^2 bonded network by adopting sp^3 hybridization, which in the dilute limit will act as an impurity or a defect in the gigantic π-network and begins to create tunable band gap in graphene.[81] In the high coverage limit, the conducting π-network becomes largely saturated, converting π and sp^2 of graphene into most sp^3 covalent bonds of graphane. Consequently, graphane was computed to be a wide gap semiconductor, with a direct band gap of 3.5–4.0 eV.[19,82] It was recently suggested that doped graphane can be a high-T_c electron–phonon superconductor.[83] Half-hydrogenated graphene was computed to have a band gap of 0.43 eV.[82] At lower coverage, chemisorbed hydrogen atoms tend to form dimers,[81,84] while at higher coverage clusters tend to form.[20]

In the intermediate regime, plenty of room is left for patterned chemisorption of hydrogen. Patterned hydrogenation was achieved by cleverly using the Moiré pattern formed between graphene and the Ir(111) surface.[85] In this experiment, graphene is placed on an Ir(111) substrate; the mismatch of lattice constants results in a geometric and electronic modulation on graphene and leads to a superlattice structure termed the Moiré pattern.[86–88] At low dosing of atomic hydrogen over graphene on Ir(111), the hydrogen coverage follows the underlying Moiré superlattice, as confirmed by the superlattice diffraction spots in the Fourier transform of the adsorption STM micrograph (see Fig. 4c). This indicates that the Moiré pattern also presents a spatial modulation of the reactivity of graphene toward hydrogenation. Angle-resolved photoemission spectroscopy (ARPES) reveals a well-defined band structure, indicative of long-range ordering of the chemisorbed hydrogen, as exemplified in Fig. 4d. The band gap opens and evolves as the hydrogen coverage increases.

This is only the beginning of playing chemical tricks on graphene. Hydrogenation or other chemical functionalization of graphene is very effective in tuning the band gap, a critical issue for electronic devices.[89] At present, it is possible to control the total coverage of graphene by hydrogen through careful dosing of the atomic hydrogen (concentration and time). But methods for producing well-defined patterns on the nanometre scale remain limited, which are essential if the goal is to produce devices with desired properties reproducibly. For example, stripes with alternating graphene and graphane can have interesting band gap modulation along with ferro- and antiferromagnetic ground states.[90] To achieve the guided formation of chemisorbed patterns, masks (broadly defined) can be introduced to block hydrogen's access to graphene in selected areas, like in spray printing. It is noted that physically blocking the access to graphene during the hydrogenation process can reduce or eliminate the hydrogenation in selected areas. In fact, by virtue of limiting the access of hydrogen by the substrate single-sided hydrogenation can be achieved, resulting in a non-crystalline structure. The mask material should have good affinity to graphene, and be easy to remove.

4. Mechanically induced patterns

In the previous sections, we examined the methods for creating patterns on graphene that involve breakage and/or formation of chemical bonds. In this section, we describe strategies of creating patterns on graphene by means of applied mechanical strain, keeping the connective covalent bonds intact. Because most physical and chemical properties of crystals depend on the lattice constant (in the case of membranes, out-of-plane bending curvatures as well), inducing a homogeneous or inhomogeneous elastic strain field can change and spatially modulate the properties, which is the idea of "elastic strain engineering" (ESE).[91] In order to achieve significant property changes by means of ESE, one often requires the material to possess a high mechanical

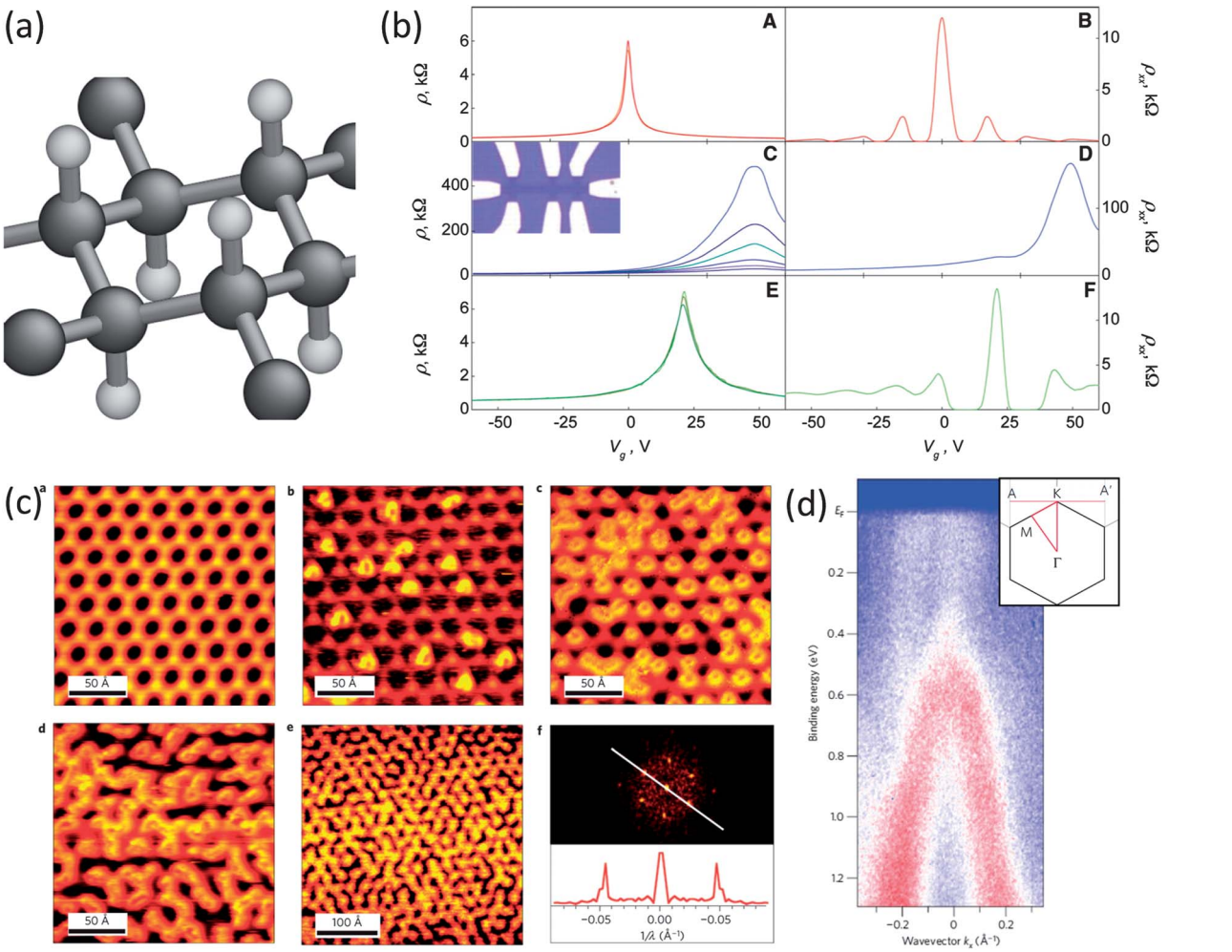

Fig. 4 (a) The structure of graphane in the chair conformation, which can be viewed as a fused cyclohexane. (b) Measured resistivity without magnetic field (ρ) at different temperatures and with magnetic field (ρ_{xx}), before hydrogenation (A and B), after hydrogenation (C and D), and after hydrogen desorption (E and F).[79] Inset, the micrograph of the typical Hall measurement setup. (c) STM micrographs of graphene with various degrees of hydrogenation (a–e), where hydrogen atoms are the bright spots or areas. Panel f is the Fourier transform of the micrograph in panel e.[85] (d) Angle-resolved photoemission intensity of hydrogenated graphene along A–K–A′ (see inset[85]). (Reprinted with permission from ref. 79, Copyright© 2009 AAAS; ref. 85, Copyright© 2010 Macmillan Publishers Ltd: *Nature Materials*.)

strength, so a significant elastic strain and stress can be imposed on the material for a long period of time without internal stress relaxation (dissipation) by plasticity or fracture. Atomically thin membranes offer unique opportunities for elastic strain engineering for the reasons outlined below.

In many 3D metallic and ceramic polycrystals, films, multilayers and wires, a "smaller is stronger" trend[91–94] has been firmly established, attributed to the confinement of the population dynamics of extended defects such as dislocations and cracks. Atomically thin membranes such as graphene and graphane can be regarded as confined dimensionally to the extreme in the normal direction, and thus can have exceptional mechanical strength. In this regard, graphene can be viewed as an example of the *ultra-strength materials*.[20,91,95] As a practical definition, an ultra-strength material can elastically withstand a sample-prevailing stress of more than one percent of its Young's modulus. It was predicted and later measured that the ideal strength (σ_I) of graphene is over 100 GPa, equivalent to an ideal strain of $\varepsilon_I = 0.25$.[20,21] The unique feature of graphene as a highly anisotropic, atomically thin membrane with ultrastrength makes it very attractive to create patterns *via* ESE.

As an example of the use of in-plane strain, the hydrogenation binding energy can be modified upon application of biaxial strain.[18] And the application of elastic strain can also significantly modify the band gap of graphane.[96] However, homogeneous strain has not resulted in qualitative change in the band structure of graphene or, especially, significant band gap opening. But what about introducing strain texture to graphene? For a more general view of strain, it has been suggested that a 2D strain field, $u_{\alpha\beta}(x,y)$ amounts to an effective gauge field,[30,97–102] written in terms of the vector potential,

$$\boldsymbol{A} = -\left(\frac{\partial \ln t}{\partial a}\right)\begin{pmatrix} u_{xx} - u_{yy} \\ -2u_{xy} \end{pmatrix} \quad (1)$$

where t is the nearest-neighbour (NN) hopping integral, and a is the lattice parameter. It is obvious that non-uniform strain fields can be thought of as a pseudomagnetic field (the time-reversal symmetry is not broken by the strain alone). For simple

homogeneous strain or any strain that results in irrational vector potential, there will be no effective magnetic field. A strain field may act like an applied magnetic field, which, however, does not violate the time-reversal symmetry as it has opposite signs at the two pseudo-spin valleys, K and K'.[101] This effective field is called the pseudo-magnetic field, $\boldsymbol{B}_s = \nabla \times \boldsymbol{A}$. Guinea *et al.* demonstrated theoretically that a nearly homogeneous magnetic field can be achieved by stretching a circular graphene membrane along the three $\langle 100 \rangle$ axes (see Fig. 5a).[99] This theoretical prediction was soon supported by Levy *et al.* through spectroscopic measurements by STM of graphene nanobubbles.[103] Landau levels were found in the highly strained graphene nanobubbles, which originate from a strain-induced pseudo-magnetic field greater than 300 Tesla. As the highest *real* magnetic field achievable in the lab is less than 100 Tesla within a period of a few milliseconds, elastic strain engineering thus provides an alternative way for the study of physics in high magnetic fields.

It was suggested that graphene is intrinsically unstable as an ideal flat 2D crystal, and the strict 2D translational symmetry is spontaneously broken due to the formation of energetically cheap ripples.[104–108] These ripples correspond to out-of-plane displacement of atoms as much as 10 Å with a spatial extent over 200 Å, depending on the boundary condition and size of graphene. It is our daily experience that thin sheets are very easy to fold or form ripples and wrinkles. Indeed, the lowest energy phonons of unstretched graphene are dominated by bending waves, which have a distinct $\omega \propto k^2$ frequency–wavevector dispersion[20] rather than the normal $\omega \propto k$ dispersion of long-wavelength phonons, indicating that the bending waves are especially floppy. The bending modulus is defined as

$$D \equiv \frac{\mathrm{d}M}{\mathrm{d}\kappa} = \frac{\sqrt{3}}{4}\frac{\partial V}{\partial \theta_{ijk}} \tag{2}$$

where M is the bending moment, and κ the curvature of the sheet. The second expression is specific for the 2D honeycomb lattice, where V is the potential energy, and θ_{ijk} is the bond angle given a 3-body interatomic potential. For a back-of-envelope estimate of the energy involved in bending ΔV per atom $\sim 4 \times 3^{1/2} D \Delta\theta \sim 4.3\ \mathrm{eV} \times \Delta\theta$, which amounts to a few tens meV for typical angular variations. It takes much less energy to bend a graphene sheet than to stretch it in order to produce similar atomic displacements. Thus, it is relatively easy to create textures on graphene by creating ripples or wrinkles. Indeed, it was found that epitaxially grown graphene on metal surfaces can also develop textured ripples due to the weak graphene–substrate interaction and the mismatch of the periodicities between graphene and the substrate (Moiré pattern).[25–27] These ripples in graphene on Ir(111) lead to minigaps in the electronic energy spectrum.[109]

The idea of creating curvature on graphene (as an atomically thin membrane), *i.e.*, ripples and wrinkles, is motivated again by the notion of deformation potential, that a strain field may enter the quantum Hamiltonian as an effective vector potential.[100–102] This is because curvature involves changing the bond angles, and consequently, the hopping matrix elements *via* rehybridization of carbon's valence orbitals, in a way similar to the vector potential in the massless Dirac equation.[100] Kim and Castro Neto showed theoretically that the local curvature on a graphene membrane (mean out-of-plane displacements ~0.5 nm) introduces a fluctuation in the local electrochemical potential on the order of ±30 meV.[110] In fact, the edge stress of graphene[111] can cause a lot of bending and ripples,[112,113] as shown in Fig. 5b.

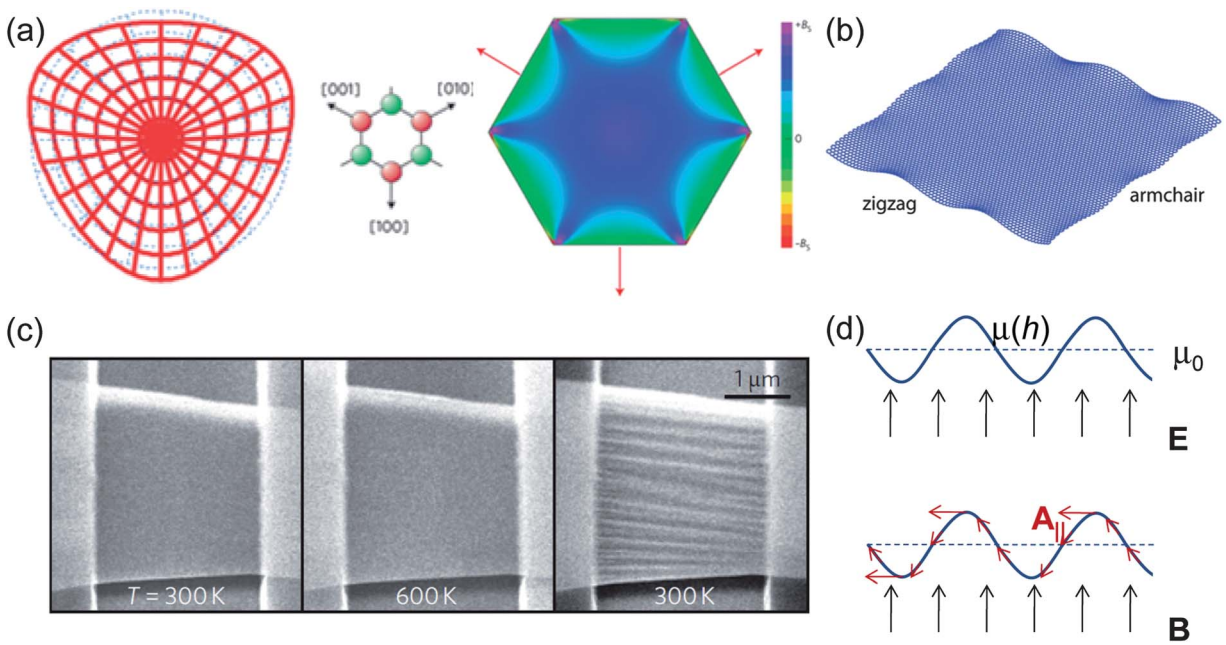

Fig. 5 (a) In-plane strain induced pseudo-magnetic field: left panel – suggested stretching of a circular graphene membrane; right panel – the resultant pseudo-magnetic field.[99] (b) Edge stress induced rippling of graphene.[112] (c) Wrinkles in few-layer graphene upon stretching.[115] (d) Combining wrinkles with external fields. (Reprinted with permission from ref. 99, Copyright© 2010 Macmillan Publishers Ltd: *Nature Physics*; ref. 112, Copyright© 2008 American Physical Society; ref. 115, Copyright© 2009 Macmillan Publishers Ltd: *Nature Nanotechnology*.)

This rippled graphene structure is a part of the large manifold of nearly degenerate, low-energy structures, and hence very hard to control (to complicate things further, the exact origin of these "spontaneous" ripples is in fact subject to some controversy; see ref. 108). Taking one step further from ripples, a wrinkled texture on graphene can be more interesting. Here by "wrinkled texture" we mean an ideally periodic arrangement along one specific direction of the out-of-plane displacement. It perhaps is helpful to think of spontaneous ripples as the glassy state, while the wrinkles as the crystalline state. It is well known in the continuum elasticity that an elastic film, subject to uniaxial tension, can develop a longitudinal wrinkled texture due to the transverse Poisson stress coupled with a nominal rigidity arising from continuity toward the clamped edges.[114] Not surprisingly, graphene does just that; it forms quasi-periodic wrinkles upon stretching (see Fig. 5c).[115,116] Compared to spontaneous ripples, wrinkles are more desirable as the wrinkles are quasi-periodic, and their periodicity and amplitudes can be tuned by adjusting the tension. As an atomically thin membrane, the atomic fluctuation in graphene is going to be important.

With pure bending, the electronic perturbation is relatively gentle, causing small effects on the electronic properties of graphene. Here we suggest that coupling the wrinkle texture with external fields may be explored for tuning the electronic properties of graphene. It is usually easy to apply uniform fields (electric or magnetic). When graphene is flat or approximately flat, it sees a uniform field. However, with the wrinkle textures, the out-of-plane displacement of carbon atoms, $h(x,y)$, modulates the field(s). In the case of a uniform vertical electric field $\boldsymbol{E} = E_z\hat{\boldsymbol{z}}$, the electrochemical potential of electrons on graphene now becomes $\mu(x, y) = E_0h(x,y) + \mu_0$, where μ_0 is the potential corresponding to zero displacement, as schematically displayed in Fig. 5d. With a gating voltage across the graphene membrane with wrinkles, charge localization can be immediately achieved. The periodicity and amplitude of the charge modulation is tunable by mechanically adjusting the applied tension, or by electrically varying the applied field.

With an applied magnetic field, $\boldsymbol{B} = B\hat{\boldsymbol{z}}$, the wrinkles enter the Schrödinger equation as a modulation on the vector potential, $\boldsymbol{A}$,

$$\boldsymbol{p} = \hbar\boldsymbol{k} - e\boldsymbol{A} \tag{3}$$

In the case of a flat graphene sheet, the vector potential in the Landau gauge is $\boldsymbol{A} = xB\hat{\boldsymbol{y}}$. Now suppose the atom positions of wrinkled graphene can be mapped on a surface, $h(x,y) = h_0\sin(qy)$. The electronic motion is still constrained along the curved surface, which, in the absence of magnetic field, is characterized by $\boldsymbol{k}$ reflecting the undeformed lattice. The vector potential, however, now has in-plane ($\boldsymbol{A}_{\|}$) and out-of-plane ($A_{\perp}$) components. And only the in-plane vector potential goes into the Schrödinger equation, as $\boldsymbol{p} = \hbar\boldsymbol{k} - e\boldsymbol{A}_{\|}$. As we can see in Fig. 5d, it is clear that now the vector potential is no longer a constant, but

$$\boldsymbol{A}_{\|} = \frac{xB\hat{\boldsymbol{y}}}{\sqrt{1 + h_0{}^2q^2\cos^2 qy}} \tag{4}$$

The effect of wrinkles can also be understood from a classical point of view. When the electron with momentum along the x-direction is subject to the magnetic field, the Lorentz force it feels is horizontal, along the y-direction. But given that the electrons can only move along the curved surface of the membrane, only the in-plane (or tangential) force exerts an influence on the motion of electrons. Alternatively, the problem now is equivalent to a flat graphene under a non-uniform magnetic field,

$$\boldsymbol{B}_{\text{eff}} = \nabla \times \boldsymbol{A}_{\|} = (1 + h_0{}^2q^2\cos^2 qy)^{-1/2}B\hat{\boldsymbol{z}} \tag{5}$$

The geometric modulation on the magnetic field is an interesting aspect to study, as it is going to have an impact on the Landau levels and quantum Hall effects. We notice that the modulation is stronger with increasing amplitudes (h_0) or decreasing wavelength ($2\pi/q$) of the wrinkles, which are again tunable.

5. Integration of flat- and curved-carbon

It has been shown that the properties of graphene depend sensitively on its edge.[3,39,40,46,117–121] It is therefore important to have good control over the structure, directionality and quality of the edge termination. For all the methods of creating nanopatterned graphene or GNRs described in Section 1, the structures of edges formed from the energetic carving processes are not atomically smooth. The native edges of monolayer graphene are characterized by dangling sp^2 bonds on the surface carbon atoms, which can have a complex magnetic structure, and may undergo complex self-passivating reconstructions.[119] The chemical nature of the edges formed in a chemical process is expected to be often not simple either. The native edge termination created in vacuum is unlikely to survive under ambient conditions where oxygen and moisture are present, as hydrogen-, hydroxyl, oxyl- or peroxyl terminations are more stable due to the elimination of dangling bonds. Depending on the partial pressures of the air environment, the edge passivation may dynamically change as well. These complications with monolayer edge termination can have a significant impact on the transport properties of graphene nanoribbons or other nanostructures when very small sizes are desired, especially because zigzag GNRs exhibit unique electronic states strongly localized along the edge.[117] The perplexing situation with the edge issue with monolayer graphene highlights the need for what is termed bilayer edges (BLE)[8] or half nanotube[122] in graphene structures.

The BLE structure is composed of one single continuously curved graphene lattice, which is folded along the edge with a 180° turn, as shown in Fig. 6a. In the case of BLEs, structurally and chemically well-defined, and atomically smooth edges arise naturally. Huang *et al.*[8] showed that an electrical current in few-layer graphene Joule heated the graphene to 2000 °C. This much heat was enough to cause the carbon atoms to sublime into the air from graphene. Open edges were formed initially, which quickly relaxed to the more stable bilayer edges to eliminate dangling bonds (Fig. 6b). Slightly before Huang *et al.*'s work, Iijima *et al.* also discovered that BLEs can be created through furnace annealing of graphite samples at 2000 °C (Fig. 6c).[123] Compared with MLEs, BLEs are chemically more inert,[123] and crystallographically better defined compared with monolayer edges.[124] Remarkably, the atomically smooth BLEs can only

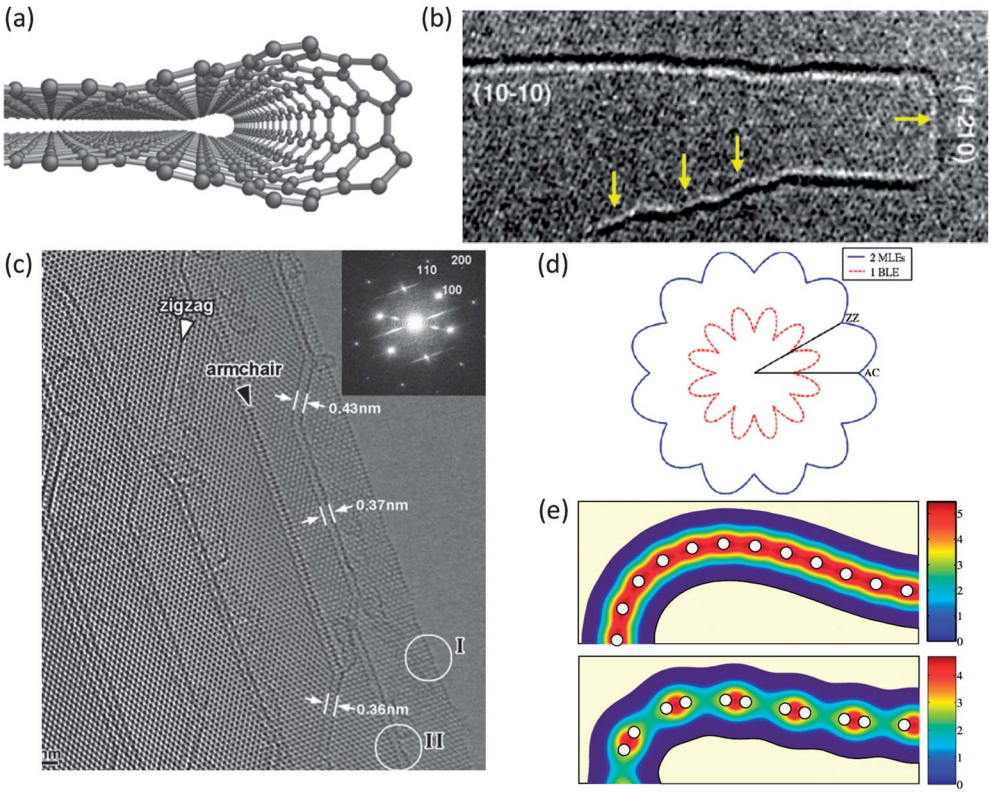

Fig. 6 (a) The atomic structure of a zigzag bilayer edge termination. (b) Transmission electron microscopic (TEM) micrograph of BLEs formed from a Joule heated sublimation process.[8] Both zigzag and armchair inclinations are observed. (c) TEM micrograph with atomic resolution of multiple BLEs formed from annealing graphite powder at 2000 °C for 3 hours.[123] (d) Semi-quantitative Wulff plots for mono- and bilayer edge terminations in a polar representation.[124] (e) Computed (density functional theory) valence electron density of armchair (top) and zigzag (bottom) BLEs, demonstrating the Coulombic relaxation of electron density from the inside of the BLE to the outer surface.[130] (Reprinted with permission from ref. 123, Copyright© 2009 American Physical Society.)

form along two crystallographic directions, to have either armchair or zigzag terminations,[8,123,124] a property certainly desirable if devices with controlled edge termination are to be made. The highly selective edge inclinations (zigzag or armchair) of BLEs correspond to deep cusps in a semi-quantitative Wulff plot for the edge energy as a function of edge inclination (Fig. 6d),[124] whereas the Wulff plot for monolayer graphene edges is much more isotropic in comparison. These advantages of BLEs make this type of terminations more suitable for creating patterns for consistent properties. Recently, graphene sheets have been used to make nanopore devices for single-molecule sensing and potential low-cost DNA sequencing applications.[125–129] The long-term stability of such a graphene nanopore device may also benefit from forming chemically inert but electronically sensitive BLE structures at the pore edge.

Geometrically, one could view a BLE as a half carbon nanotube (folding graphene by π), only now without the left–right symmetry of the full nanotubes (folding graphene by 2π). As a result of the missing symmetry, the BLEs can develop spontaneous electric dipole due to Coulombic relaxation of the electronic density upon bending,[130] and rehybridization of the pπ bonds.[131] First-principles calculations show that BLEs possess extensive electric dipoles along the edges, on the order of $\sim$1.3 debye Å^{-1} (see Fig. 6e). BLE terminations also mechanically enforce AA stacking[123] to the bilayer graphene connected to them, which leads to a new class of quantum hall effect resonance.[130]

One point associated with Joule heating derived nanostructures is that there is a wide variety of carbon nanostructures generated simultaneously as an integral part of the mother graphene structures. We thus take one step further to suggest that there might be a possibility of integrating flat carbon (graphene) with curved carbon (nanotubes and half nanotubes) in a single device. Like flat graphene, carbon nanotubes (CNT) possess many attractive physical properties. In particular, semiconducting single-wall carbon nanotubes (SWCNTs) with appropriate diameter and chirality can have a significant electronic energy gap[100,132] (Kataura plot) comparable to that of silicon, 1.1 eV, which is necessary for making room-temperature electronic logical devices with large on–off ratio in current. Such an appropriate gap, however, is absent in unconfined graphene. SWCNTs also have excellent transport properties.[133] Indeed, better-than-silicon device characteristics have been demonstrated for certain SWCNT devices at an individual device–element level.[134]

The major issue with using CNTs in practice, however, is with the assembly process and device behaviour reproducibility. Carbon nanotubes are structurally polydisperse, as SWCNTs with different chirality and diameters are nearly degenerate in formation energy and often coexist from various synthetic routes. In a typical preparative process, after growing the nanotubes somewhere (for instance arc-discharge or CVD chamber), one needs to take them out, sort them,[135] cut,

manipulate, and orient one on a substrate, and then interface with metallization electrode materials, using for instance ion-beam deposition. This device assembly process is time-consuming, far from automated/scalable. The performance of a device so-prepared is often detrimentally nonuniform due to the polydispersity of nanotubes. It also suffers from uncontrolled metal–carbon atomic contact at the electrode interface.

In a recent work from some of us,[122] we proposed a novel device architecture, composed of carbon nanotube–graphene hybrids. This design is inspired by Huang *et al.*'s *in situ* observation of BLE (half nanotube) formation, where a multitude of coherently connected graphene, BLE and nanotube structures have been observed.[8,38,124] In particular, TEM indicates that single-wall carbon nanotubes can be connected to BLE[8,123,130] and bridge few layers of flat graphene, as shown in Fig. 7A–E; similar nanotube bridge structures were also fabricated by high-temperature (>600 °C) electron beam irradiation of few-layer graphene.[37] Our molecular simulations further demonstrated the possibility of formation of such nanotube–graphene hybrids in a controllable manner by lithographic cutting and self-folding of graphene, illustrated in Fig. 7F. The self-folded semiconducting nanotubes and semi-metallic graphene form a "metal–semiconductor–metal" junction. The calculated electronic conductance spectrum of such a metal–semiconductor–metal junction indicates that the intrinsic transport gap of the nanotube (when it is infinitely long), 0.8 eV, is preserved (see Fig. 7I) in spite of the presence of four geometrically necessary disinclination defects at the interface between flat carbon and curved carbon. This is the best outcome one could hope for.

It is worth noting that the device fabrication concept above differs from traditional nanotube-based devices in two important ways. First, the device is made entirely out of carbon, all sp^2 carbon in fact. No other elements are necessary as electrodes, since flat graphene is already a reasonable transparent electrode

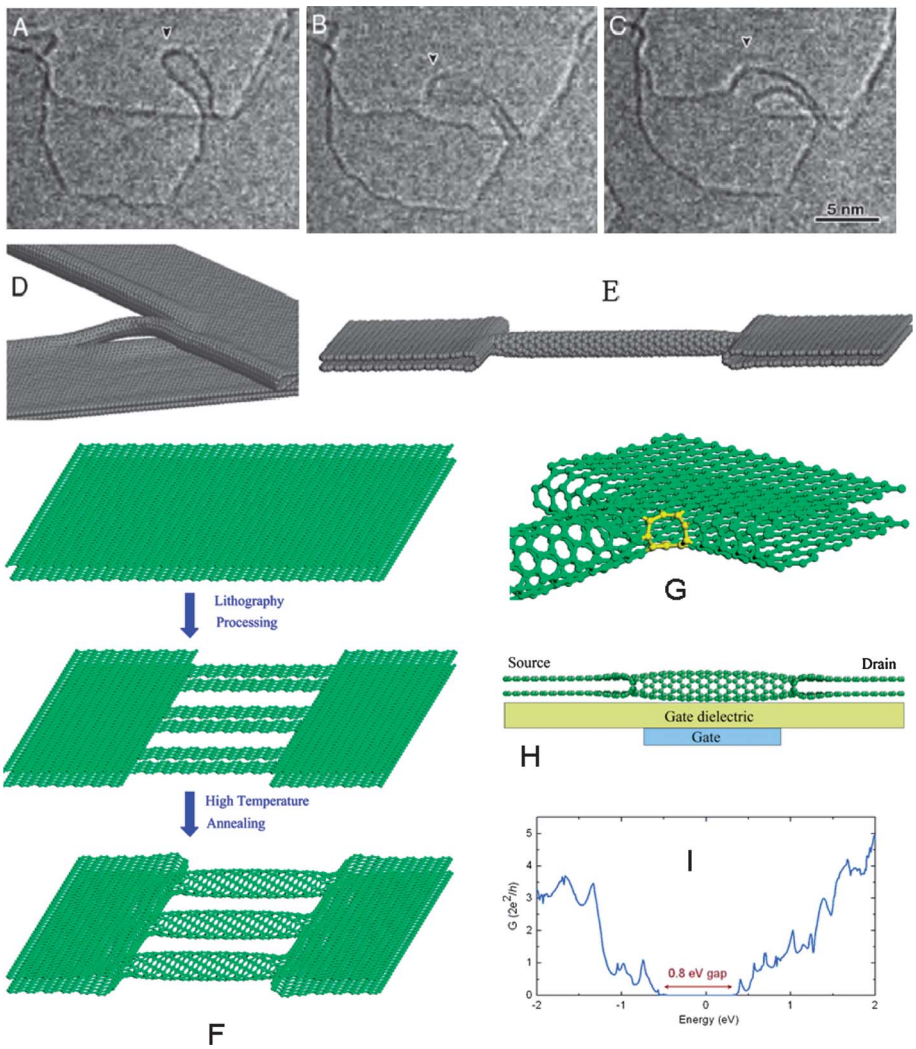

Fig. 7 Carbon nanostructures formed *in situ* on graphene substrate by Joule-heating. A–C show two neighboring bilayer graphenes interconnected by a carbon nanotube, as pointed out by the arrowheads. D, E, F and G are atomic structural models. Panel F shows one possible patterning process, supported by MD simulation.[122] In G we can see a nine-sided polygon, highlighted in yellow, amidst the hexagonal bonding network of graphene, which is a geometrical disinclination at the interface between flat and curved carbon. H shows a FET device model (side view) based on single-wall carbon nanotube and bilayer graphene hybrids. Panel I shows the calculated electronic conductance spectrum of the metal–semiconductor–metal (flat graphene–nanotube–flat graphene) junction device,[122] where the intrinsic transport gap of the nanotube is preserved.

material.[59,136] The uncertainty with the geometric and electronic states of monolayer graphene edges is avoided by self-wrapping to form curved SWCNTs and BLEs. Such a coherent junction of flat carbon and curved carbon[8] possesses high physical and chemical inertness as carbon nanotubes and fullerenes, and so the device behaviour should not change with the gas environment at near room temperature. Second, the way our devices would be assembled (*e.g.* cutting and self-folding at high temperatures) differs fundamentally from the traditional two-step approaches in which growth (for instance arc-discharge or CVD chamber) and assembly of carbon nanotubes are carried out at two different locations. The self-folded structures were created by cutting graphene,[8,38,124] which then curls up due to edge stress and thermal fluctuations, and fuses together, while maintaining connection to the mother graphene. Therefore, minimal subsequent processing or electrification is necessary. The *in situ* assembly approach is only possible in 2D layered materials where bending is easy, analogous to factory workers working on sheet metals. Consequently, SWCNTs can be fabricated directly into device structures and even integrated circuits by a process of cutting few-layer graphene, followed by proper thermal annealing to allow self-folding. The temperature of the annealing stage must be well controlled and programmed: it must be high enough to allow edge diffusion of carbon atoms to accomplish the folding reconstruction and anneal away geometrically unnecessary defects (the geometrically necessary defects like those in Fig. 7G can never be annealed away, so there is a minimum number of them). But it cannot be too high to induce unwanted sublimation.[8] Our preliminary molecular simulations indicate that such an intermediate temperature can indeed be found.[122]

The experimental realization of the above vision of fabricating devices with an all-carbon architecture depends critically on proper patterning of graphene, which is the central theme of the current review. Although formation of defect-free nanotubes and/or half nanotubes (BLEs) from graphene may require patterning techniques with atomic resolution, we believe that existing techniques such as scanning probe lithography,[40–42] helium ion beam lithography,[43] and electron beam lithography[35] qualify for a proof-of-concept experiment. The characteristics, strength and limitations of these techniques are reviewed earlier in this paper.

6. Programming graphene origami (folding) by kirigami (cutting)

In 1995, carbon nanotube pioneers Ebbesen and Hiura wrote a visionary article "Graphene in 3-Dimensions: toward graphite origami".[33] Ebbesen and Hiura, noting graphene's out-of-plane flexibility, imagined that graphene could be folded to give rise to a variety of shapes, reminiscent of Japanese paper folding game known as origami. If paper cutting is further allowed, the game is elevated to the next level called kirigami. Ebbesen and Hiura proposed that cutting well-defined shapes in two or more layers of graphene, followed by annealing, would "allow one to design nanotubes with a given diameter and perhaps even helicity". Huang *et al.*'s *in situ* experiments on multi-layer graphene[8,38,124] proved that their vision is valid. Indeed, the rich topologies formed in Huang *et al.*'s kirigami experiments (Fig. 7A–D) have led us to believe that graphene provides a basis for "plumber's wonderland", where large folding in 3D could be *prescribed* by precise cutting and annealing.

What is the most exciting trick one can do with a precise patterning tool? One may interpret patterning as writing *information* on a 2D sheet. By regarding graphene kirigami as *encoding* a set of instructions on how to fold, we may emulate how Biology encodes genetic information. Indeed, "programmable matter" is Biology's trick to create a world so lively and varied (Fig. 8a). Information is encoded in the amino acid sequence of a protein, which guides the long-chain polymer to fold into very complex secondary and tertiary structures in solution with highly specific functionalities. This genetic information can also be replicated many times with small errors, and the outcome of the folding program is highly deterministic. In other words, starting from different random states and impacted by the random forces in the solution, the protein can nonetheless fold into its native state surprisingly quickly (usually on ms or μs timescale), side-stepping the so-called Levinthal's "paradox" in traversing an energy landscape.[137] In proteins such extremely accurate and rapid folding is accomplished by an evolutionary "design" of the folding energy landscape that arises from weak interactions of electrostatic/hydrogen-bond, van der Waals and elastic energies, which are an order of magnitude weaker than the primary bonds (see also our Table 1).

Like proteins, graphene has weak interactions from van der Waals interactions and bending elastic energy. Surprisingly, it can also have weak electrostatic interactions. Recent experiments have resolved the atomic structures of BLEs (half nanotubes),[8,123,124,130] which we have discussed earlier in this review (Fig. 8b). BLEs are theoretically predicted to have significant electric dipole moments, 0.87 and 1.14 debye $Å^{-1}$ for zigzag (ZZ) and armchair (AC) inclinations, respectively.[130] A ring of BLE enclosing vacuum on bilayer graphene forms the so-called bilayer pore (BLP). Due to the difference in the dipole magnitude between ZZ and AC BLEs, a triangular BLP composed of two AC BLEs and a ZZ BLE would result in a net dipole of $\sim 0.3 \times l$ debye, where l is the base length (Å) of the triangular unit (Fig. 8c). Even though graphene is a semimetal and in-plane partial screening of the electric field will occur, each triangular BLP would possess significant electric dipole.

Thus atomic membranes like graphene possess the same arsenal of weak forces as proteins: electrostatic, van der Waals and elastic energies. Our preliminary molecular simulations also indicate that the BLEs are polar and hydrophilic, while away from BLEs the flat graphene is aromatic and hydrophobic. So with precise patterning of flat graphene, we may in principle write 2D folding programs on graphene using different BLPs, just like Biology writes 1D folding programs on DNA/protein molecules using A-C-G-Ts and 21 amino acids. We envision a 3-step process: (1) BLPs of different sizes, shapes, orientations and positions are encoded on graphene by kirigami on an "operating table", where the sample stays essentially flat due to clamping on the boundary of a hole, or adhesion to a substrate; then (2) a temperature-annealing step will be performed (Section 4) to achieve local nanoscopic curvatures and topological reconstructions (Fig. 7F), so BLEs and nanotubes can form, but the overall sample shape is still flat; and in (3), the sample is released into solution or air: the bending stiffness will be overcome by a combination of thermal fluctuations, electrostatic interactions

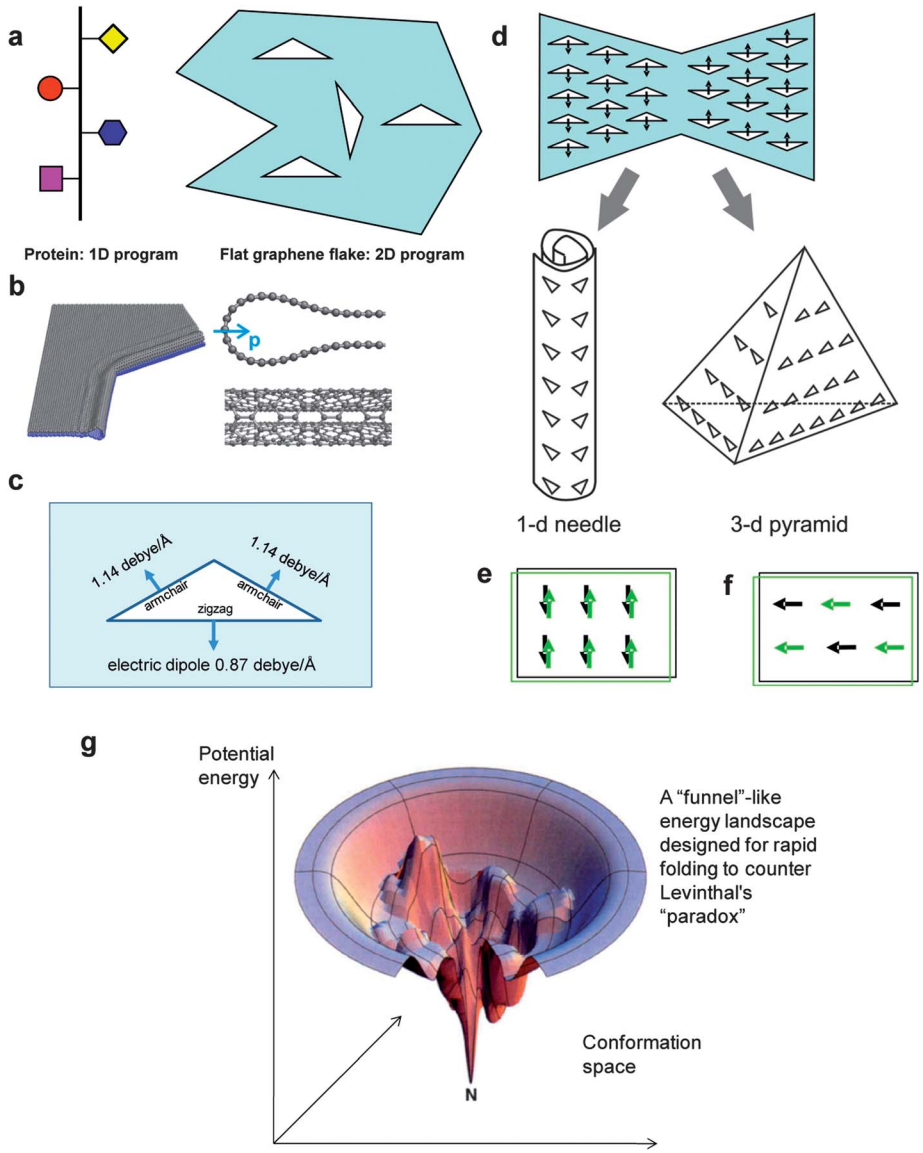

Fig. 8 (a) Programmable matter. (b) Structure of BLE (left) and side/front view of a BLE (right). (c) A triangular bilayer pore (BLP) consisting of 3 BLEs. Zigzag and armchair BLEs have permanent electric dipoles of 0.87 and 1.14 Debye $Å^{-1}$, respectively. This difference leads to a net dipole of ~0.3 × *l* debye in the structure, where *l* is the base length (Å) of the BLP. (d–f) Programmed folding of a BLE membrane. Maximization of attractive dipole–dipole interaction could guide graphene membrane folding into complex structures. (g) Illustration of the folding energy landscape, with N being the desired 3D conformation or the native state.[137] (Reprinted with permission from ref. 137, Copyright© 1997 Macmillan Publishers Ltd: *Nature Structural Biology*.)

and van der Waals adhesion, and the whole sample starts to fold in earnest, and a 3D structure shall arise out of a 2D "program". We note that with only van der Waals interactions, a large piece of free-standing graphene would prefer to fold many times to maximize the adhesion. But van der Waals interactions are quite isotropic and purely attractive. Having directional (anisotropic) dipole–dipole electrostatic forces[130] with the possibility of repulsion gives one a lot more design freedoms.

We may envision several outcomes of such programmable folding. In the first, the membrane may fold in 3D like in origami. In order to fold the bilayer membrane along a specific line we desire, the membrane could be tailored such that it has a line along which the bending stiffness is particularly small. First, when the membrane has a very narrow region the bending stiffness across that region will be correspondingly small, such as the shape of a bowtie as shown in Fig. 8d. Second, we can carve out one layer of the bilayer membrane along a line of choice to reduce the bending stiffness, and also remove the BLE at two ends of the line. This needs to be done at low temperature with an AFM tip so that the fresh monolayer edges do not anneal. The membrane could be designed such that upon folding, it goes into some 3-D structure, such as the pyramid shown in Fig. 8d.

In the second, the membrane may roll up into a 1-D wire like a tobacco leaf rolling into a cigar (Fig. 8d). We can design the dipole pattern on the graphene membrane to control the chirality of folding and net dipole. If the dipoles from adjacent membranes are coupled antiparallel, then there is a net cancellation of dipoles (Fig. 8e). But if the dipoles are aligned in a

head-to-tail fashion, the folded structure will have an overall dipole (Fig. 8f). It would be a very interesting theoretical problem how the chirality of folding is controlled by the patterning of a BLP array with net electric dipoles.

In summary, graphene has opened up a kirigami and origami wonderland, where many exciting topologies and architectures[8,38,124] could be designed. Just like a protein's 1D program of 21 amino acids, we may one day write 2D programs on flat graphene by for example encoding the size, shape, orientation and position of BLPs, to guide deterministic graphene folding in solution or air. Again, we emphasize the crucial role of precise patterning. Biology's molecular machineries (RNA polymerase, ribosome, *etc.*) allow nearly error-free transcription, translation and execution of the folding program, utilizing weak or "soft" forces to control secondary/tertiary structures of proteins. To achieve a similar degree of sophistication and precise determinism, we must enhance the reproducibility of graphene patterning: that is, repeated experimental instances of purportedly the same lithographic design must actually result in nearly identical patterns. Also, one must learn from the science of protein folding to design both the thermodynamic end point of folding as well as facile kinetics of folding, for example by designing a "funnel"-like energy landscape (Fig. 8g), to sidestep Levinthal's paradox and achieve rapid and deterministic folding.[137] Glassy dynamics[138] in folding must be avoided.

7. Outlook

As a final word, we again take a historical perspective. In 1910, Johannes van der Waals won the Nobel Prize for one "simple" thing he did. He wrote with his pencil on a piece of paper the ideal gas equation of state, with two extra constants. 100 years later, Andre Geim and Kostya Novoselov won the Nobel Prize, and again for one "simple" thing they did. They took out their pencil, but decided to write on a scotch tape.

Acknowledgements

We appreciate helpful discussions with Jianyu Huang, and acknowledge support by NSF DMR-1120901 and AFOSR FA9550-08-1-0325. J.F. acknowledges the support from NSFC (Project 11174009).

References

1 K. S. Novoselov, D. Jiang, F. Schedin, T. J. Booth, V. V. Khotkevich, S. V. Morozov and A. K. Geim, *Proc. Natl. Acad. Sci. U. S. A.*, 2005, **102**, 10451–10453.
2 F. Miao, S. Wijeratne, Y. Zhang, U. C. Coskun, W. Bao and C. N. Lau, *Science*, 2007, **317**, 1530–1533.
3 Y.-W. Son, M. L. Cohen and S. G. Louie, *Phys. Rev. Lett.*, 2006, **97**, 216803.
4 X. Li, X. Wang, L. Zhang, S. Lee and H. Dai, *Science*, 2008, **319**, 1229–1232.
5 V. Barone, O. Hod and G. E. Scuseria, *Nano Lett.*, 2006, **6**, 2748–2754.
6 F. Banhart, *Rep. Prog. Phys.*, 1999, **62**, 1181–1221.
7 L. Sun, F. Banhart, A. V. Krasheninnikov, J. A. Rodriguez-Manzo, M. Terrones and P. M. Ajayan, *Science*, 2006, **312**, 1199–1202.
8 J. Y. Huang, F. Ding, B. I. Yakobson, P. Lu, L. Qi and J. Li, *Proc. Natl. Acad. Sci. U. S. A.*, 2009, **106**, 10103–10108.
9 D. R. Nelson, T. Piran and S. Weinberg, *Statistical Mechanics of Membranes and Surfaces*, World Scientific Pub, River Edge, N.J, 2004.
10 S. A. Safran, *Statistical Thermodynamics of Surfaces, Interfaces, and Membranes*, Addison-Wesley Pub, Reading, Mass, 1994.
11 C. O. Girit, J. C. Meyer, R. Erni, M. D. Rossell, C. Kisielowski, L. Yang, C.-H. Park, M. F. Crommie, M. L. Cohen, S. G. Louie and A. Zettl, *Science*, 2009, **323**, 1705–1708.
12 B. W. Smith and D. E. Luzzi, *J. Appl. Phys.*, 2001, **90**, 3509–3515.
13 V. K. Tewary and B. Yang, *Phys. Rev. B: Condens. Matter Mater. Phys.*, 2009, **79**, 075442.
14 L. A. Girifalco and R. A. Lad, *J. Chem. Phys.*, 1956, **25**, 693–697.
15 L. A. Girifalco and M. Hodak, *Phys. Rev. B: Condens. Matter Mater. Phys.*, 2002, **65**, 125404.
16 J. C. Charlier, X. Gonze and J. P. Michenaud, *Europhys. Lett.*, 1994, **28**, 403.
17 J. S. Arellano, L. M. Molina, A. Rubio and J. A. Alonso, *J. Chem. Phys.*, 2000, **112**, 8114–8119.
18 K. Xue and Z. P. Xu, *Appl. Phys. Lett.*, 2010, **96**, 063103.
19 J. O. Sofo, A. S. Chaudhari and G. D. Barber, *Phys. Rev. B: Condens. Matter Mater. Phys.*, 2007, **75**, 153401.
20 F. Liu, P. M. Ming and J. Li, *Phys. Rev. B: Condens. Matter Mater. Phys.*, 2007, **76**, 064120.
21 C. Lee, X. D. Wei, J. W. Kysar and J. Hone, *Science*, 2008, **321**, 385–388.
22 R. Nicklow, N. Wakabayashi and H. G. Smith, *Phys. Rev. B: Condens. Matter Mater. Phys.*, 1972, **5**, 4951.
23 L. Qiang, M. Arroyo and R. Huang, *J. Phys. D: Appl. Phys.*, 2009, **42**, 102002.
24 A. K. Geim and K. S. Novoselov, *Nat. Mater.*, 2007, **6**, 183–191.
25 M. J. Allen, V. C. Tung and R. B. Kaner, *Chem. Rev.*, 2010, **110**, 132–145.
26 A. K. Geim, *Science*, 2009, **324**, 1530–1534.
27 C. N. R. Rao, A. K. Sood, K. S. Subrahmanyam and A. Govindaraj, *Angew. Chem., Int. Ed.*, 2009, **48**, 7752–7777.
28 A. K. Geim and A. H. MacDonald, *Phys. Today*, 2007, **60**, 35–41.
29 M. I. Katsnelson, *Mater Today*, 2006, **10**, 20–27.
30 A. H. Castro Neto, F. Guinea, N. M. R. Peres, K. S. Novoselov and A. K. Geim, *Rev. Mod. Phys.*, 2009, **81**, 109–162.
31 S. Park and R. S. Ruoff, *Nat. Nanotechnol.*, 2009, **4**, 217–224.
32 D. Wei and Y. Liu, *Adv. Mater.*, 2010, **22**, 3225–3241.
33 T. W. Ebbesen and H. Hiura, *Adv. Mater.*, 1995, **7**, 582–586.
34 Z. W. Shi, R. Yang, L. C. Zhang, Y. Wang, D. H. Liu, D. X. Shi, E. G. Wang and G. Y. Zhang, *Adv. Mater.*, 2011, **23**, 3061.
35 M. D. Fischbein and M. Drndić, *Appl. Phys. Lett.*, 2008, **93**, 3.
36 J. C. Meyer, C. O. Girit, M. F. Crommie and A. Zettl, *Appl. Phys. Lett.*, 2008, **92**, 123110.
37 B. Song, G. F. Schneider, Q. Xu, G. Pandraud, C. Dekker and H. Zandbergen, *Nano Lett.*, 2011, **11**, 2247–2250.
38 J. Y. Huang, L. Qi and J. Li, *Nano Res.*, 2010, **3**, 43–50.
39 Z. Chen, Y.-M. Lin, M. J. Rooks and P. Avouris, *Phys. E*, 2007, **40**, 228–232.
40 L. Tapaszto, G. Dobrik, P. Lambin and L. P. Biro, *Nat. Nanotechnol.*, 2008, **3**, 397–401.
41 R. L. McCarley, S. A. Hendricks and A. J. Bard, *J. Phys. Chem.*, 1992, **96**, 10089–10092.
42 H. F. Hiura, *Appl. Surf. Sci.*, 2004, **222**, 374–381.
43 M. C. Lemme, D. C. Bell, J. R. Williams, L. A. Stern, B. W. H. Baugher, P. Jarillo-Herrero and C. M. Marcus, *ACS Nano*, 2009, **3**, 2674–2676.
44 D. C. Bell, M. C. Lemme, L. A. Stern, J. Rwilliams and C. M. Marcus, *Nanotechnology*, 2009, **20**, 455301.
45 L. M. Zhang, S. O. Diao, Y. F. Nie, K. Yan, N. Liu, B. Y. Dai, Q. Xie, A. Reina, J. Kong and Z. F. Liu, *J. Am. Chem. Soc.*, 2011, **133**, 2706–2713.
46 M. Y. Han, B. Özyilmaz, Y. Zhang and P. Kim, *Phys. Rev. Lett.*, 2007, **98**, 206805.
47 J. W. Bai, X. F. Duan and Y. Huang, *Nano Lett.*, 2009, **9**, 2083–2087.
48 J. W. Bai, X. Zhong, S. Jiang, Y. Huang and X. F. Duan, *Nat. Nanotechnol.*, 2010, **5**, 190–194.
49 T. Kim, H. Kirn, S. W. Kwon, Y. Kim, W. K. Park, D. H. Yoon, A. R. Jang, H. S. Shin, K. S. Suh and W. S. Yang, *Nano Lett.*, 2012, **12**, 743–748.

50 A. Sinitskii and J. M. Tour, *J. Am. Chem. Soc.*, 2010, **132**, 14730–14732.
51 S. S. Datta, D. R. Strachan, S. M. Khamis and A. T. C. Johnson, *Nano Lett.*, 2008, **8**, 1912–1915.
52 L. Ci, Z. P. Xu, L. L. Wang, W. Gao, F. Ding, K. F. Kelly, B. I. Yakobson and P. M. Ajayan, *Nano Res.*, 2008, **1**, 116–122.
53 A. Tomita and Y. Tamai, *J. Phys. Chem.*, 1974, **78**, 2254–2258.
54 A. Dimiev, D. V. Kosynkin, A. Sinitskii, A. Slesarev, Z. Z. Sun and J. M. Tour, *Science*, 2011, **331**, 1168–1172.
55 D. V. Kosynkin, A. L. Higginbotham, A. Sinitskii, J. R. Lomeda, A. Dimiev, B. K. Price and J. M. Tour, *Nature*, 2009, **458**, 872.
56 L. Jiao, L. Zhang, X. Wang, G. Diankov and H. Dai, *Nature*, 2009, **458**, 877–880.
57 L. Y. Jiao, X. R. Wang, G. Diankov, H. L. Wang and H. J. Dai, *Nat. Nanotechnol.*, 2010, **5**, 321–325.
58 X. G. Liang, Y. S. Jung, S. W. Wu, A. Ismach, D. L. Olynick, S. Cabrini and J. Bokor, *Nano Lett.*, 2010, **10**, 2454–2460.
59 K. S. Kim, Y. Zhao, H. Jang, S. Y. Lee, J. M. Kim, K. S. Kim, J.-H. Ahn, P. Kim, J.-Y. Choi and B. H. Hong, *Nature*, 2009, **457**, 706–710.
60 X. Y. Yang, X. Dou, A. Rouhanipour, L. J. Zhi, H. J. Räder and K. Müllen, *J. Am. Chem. Soc.*, 2008, **130**, 4216.
61 J. M. Cai, P. Ruffieux, R. Jaafar, M. Bieri, T. Braun, S. Blankenburg, M. Muoth, A. P. Seitsonen, M. Saleh, X. L. Feng, K. Müllen and R. Fasel, *Nature*, 2010, **466**, 470–473.
62 M. Treier, C. A. Pignedoli, T. Laino, R. Rieger, K. Müllen, D. Passerone and R. Fasel, *Nat. Chem.*, 2011, **3**, 61–67.
63 M. Sprinkle, M. Ruan, Y. Hu, J. Hankinson, M. Rubio-Roy, B. Zhang, X. Wu, C. Berger and W. A. de Heer, *Nat. Nanotechnol.*, 2010, **5**, 727–731.
64 H. L. Wang, X. R. Wang, X. L. Li and H. J. Dai, *Nano Res.*, 2009, **2**, 336–342.
65 T. Y. Kim, S. W. Kwon, S. J. Park, D. H. Yoon, K. S. Suh and W. S. Yang, *Adv. Mater.*, 2011, **23**, 2734–2738.
66 B. Li, X. T. Zhang, X. H. Li, L. Wang, R. Y. Han, B. B. Liu, W. T. Zheng, X. L. Li and Y. C. Liu, *Chem.Commun.*, 2010, **46**, 3499–3501.
67 J. M. Mativetsky, E. Treossi, E. Orgiu, M. Melucci, G. P. Veronese, P. Samori and V. Palermo, *J. Am. Chem. Soc.*, 2010, **132**, 14130–14136.
68 V. Strong, S. Dubin, M. F. El-Kady, A. Lech, Y. Wang, B. H. Weiller and R. B. Kaner, *ACS Nano*, 2012, **6**, 1395–1403.
69 M. F. El-Kady, V. Strong, S. Dubin and R. B. Kaner, *Science*, 2012, **335**, 1326–1330.
70 Y. L. Zhang, Q. D. Chen, H. Xia and H. B. Sun, *Nano Today*, 2010, **5**, 435–448.
71 L. Guo, R. Q. Shao, Y. L. Zhang, H. B. Jiang, X. B. Li, S. Y. Xie, B. B. Xu, Q. D. Chen, J. F. Song and H. B. Sun, *J. Phys. Chem. C*, 2012, **116**, 3594–3599.
72 X. Y. Cui, R. K. Zheng, Z. W. Liu, L. Li, B. Delley, C. Stampfl and S. P. Ringer, *Phys. Rev. B: Condens. Matter Mater. Phys.*, 2011, **84**, 125410.
73 A. Chuvilin, U. Kaiser, E. Bichoutskaia, N. A. Besley and A. N. Khlobystov, *Nat. Chem.*, 2010, **2**, 450–453.
74 A. A. Tseng, A. Notargiacomo and T. P. Chen, *J. Vac. Sci. Technol., B: Microelectron. Nanometer Struct.–Process., Meas., Phenom.*, 2005, **23**, 877–894.
75 C. Vieu, F. Carcenac, A. Pepin, Y. Chen, M. Mejias, A. Lebib, L. Manin-Ferlazzo, L. Couraud and H. Launois, *Appl. Surf. Sci.*, 2000, **164**, 111–117.
76 L. Bulut and R. H. Hurt, *Adv. Mater.*, 2010, **22**, 337.
77 Z. Q. Wei, D. B. Wang, S. Kim, S. Y. Kim, Y. K. Hu, M. K. Yakes, A. R. Laracuente, Z. T. Dai, S. R. Marder, C. Berger, W. P. King, W. A. de Heer, P. E. Sheehan and E. Riedo, *Science*, 2010, **328**, 1373–1376.
78 Y. L. Guo, C. A. Di, H. T. Liu, J. A. Zheng, L. Zhang, G. Yu and Y. Q. Liu, *ACS Nano*, 2010, **4**, 5749–5754.
79 D. C. Elias, R. R. Nair, T. M. G. Mohiuddin, S. V. Morozov, P. Blake, M. P. Halsall, A. C. Ferrari, D. W. Boukhvalov, M. I. Katsnelson, A. K. Geim and K. S. Novoselov, *Science*, 2009, **323**, 610–613.
80 P. Sessi, J. R. Guest, M. Bode and N. P. Guisinger, *Nano Lett.*, 2009, **9**, 4343–4347.
81 L. A. Chernozatonskii, P. B. Sorokin, E. E. Belova, J. Bruning and A. S. Fedorov, *JETP Lett.*, 2007, **85**, 77–81.
82 J. Zhou, M. M. Wu, X. Zhou and Q. Sun, *Appl. Phys. Lett.*, 2009, **95**, 103108.
83 G. Savini, A. C. Ferrari and F. Giustino, *Phys. Rev. Lett.*, 2010, **105**, 037002.
84 R. Balog, B. Jørgensen, J. Wells, E. Lægsgaard, P. Hofmann, F. Besenbacher and L. Hornekær, *J. Am. Chem. Soc.*, 2009, **131**, 8744–8745.
85 R. Balog, B. Jørgensen, L. Nilsson, M. Andersen, E. Rienks, M. Bianchi, M. Fanetti, E. Lægsgaard, A. Baraldi, S. Lizzit, Z. Sljivancanin, F. Besenbacher, B. Hammer, T. G. Pedersen, P. Hofmann and L. Hornekær, *Nat. Mater.*, 2010, **9**, 315–319.
86 A. T. N'Diaye, J. Coraux, T. N. Plasa, C. Busse and T. Michely, *New J. Phys.*, 2008, **10**, 043033.
87 A. T. N'Diaye, S. Bleikamp, P. J. Feibelman and T. Michely, *Phys. Rev. Lett.*, 2006, **97**, 215501.
88 J. Coraux, A. T. N'Diaye, C. Busse and T. Michely, *Nano Lett.*, 2008, **8**, 565–570.
89 Z. Z. Sun, C. L. Pint, D. C. Marcano, C. G. Zhang, J. Yao, G. D. Ruan, Z. Yan, Y. Zhu, R. H. Hauge and J. M. Tour, *Nat. Commun.*, 2011, **2**, 559.
90 A. K. Singh and B. I. Yakobson, *Nano Lett.*, 2009, **9**, 1540–1543.
91 T. Zhu and J. Li, *Prog. Mater. Sci.*, 2010, **55**, 710–757.
92 S. Suresh and J. Li, *Nature*, 2008, **456**, 716–717.
93 Q. Yu, Z. W. Shan, J. Li, X. X. Huang, L. Xiao, J. Sun and E. Ma, *Nature*, 2010, **463**, 335–338.
94 L. Huang, Q. J. Li, Z. W. Shan, J. Li, J. Sun and E. Ma, *Nat. Commun.*, 2011, **2**, 547.
95 T. Zhu, J. Li, S. Ogata and S. Yip, *MRS Bull.*, 2009, **34**, 167–172.
96 M. Topsakal, S. Cahangirov and S. Ciraci, *Appl. Phys. Lett.*, 2010, **96**, 091912–091913.
97 H. Suzuura and T. Ando, *Phys. Rev. B: Condens. Matter Mater. Phys.*, 2002, **65**, 235412.
98 J. L. Manes, *Phys. Rev. B: Condens. Matter Mater. Phys.*, 2007, **76**, 045430.
99 F. Guinea, M. I. Katsnelson and A. K. Geim, *Nat. Phys.*, 2010, **6**, 30–33.
100 C. L. Kane and E. J. Mele, *Phys. Rev. Lett.*, 1997, **78**, 1932.
101 S. V. Morozov, K. S. Novoselov, M. I. Katsnelson, F. Schedin, L. A. Ponomarenko, D. Jiang and A. K. Geim, *Phys. Rev. Lett.*, 2006, **97**, 016801.
102 A. F. Morpurgo and F. Guinea, *Phys. Rev. Lett.*, 2006, **97**, 196804.
103 N. Levy, S. A. Burke, K. L. Meaker, M. Panlasigui, A. Zettl, F. Guinea, A. H. C. Neto and M. F. Crommie, *Science*, 2010, **329**, 544–547.
104 N. D. Mermin, *Phys. Rev.*, 1968, **176**, 250–254.
105 J. C. Meyer, A. K. Geim, M. I. Katsnelson, K. S. Novoselov, T. J. Booth and S. Roth, *Nature*, 2007, **446**, 60–63.
106 J. C. Meyer, A. K. Geim, M. I. Katsnelson, K. S. Novoselov, D. Obergfell, S. Roth, C. Girit and A. Zettl, *Solid State Commun.*, 2007, **143**, 101–109.
107 A. Fasolino, J. H. Los and M. I. Katsnelson, *Nat. Mater.*, 2007, **6**, 858–861.
108 R. C. Thompson-Flagg, M. J. B. Moura and M. Marder, *Europhys. Lett.*, 2009, **85**, 46002.
109 I. Pletikosic, M. Kralj, P. Pervan, R. Brako, J. Coraux, A. T. N'Diaye, C. Busse and T. Michely, *Phys. Rev. Lett.*, 2009, **102**, 056808.
110 E.-A. Kim and A. H. Castro Neto, *Europhys. Lett.*, 2008, **84**, 57007.
111 S. Huang, S. L. Zhang, T. Belytschko, S. S. Terdalkar and T. Zhu, *J. Mech. Phys. Solids*, 2009, **57**, 840–850.
112 V. B. Shenoy, C. D. Reddy, A. Ramasubramaniam and Y. W. Zhang, *Phys. Rev. Lett.*, 2008, **101**, 245501.
113 K. Bets and B. Yakobson, *Nano Res.*, 2009, **2**, 161–166.
114 E. Cerda and L. Mahadevan, *Phys. Rev. Lett.*, 2003, **90**, 074302.
115 W. Bao, F. Miao, Z. Chen, H. Zhang, W. Jang, C. Dames and C. N. Lau, *Nat. Nanotechnol.*, 2009, **4**, 562–566.
116 C. Y. Wang, K. Mylvaganam and L. C. Zhang, *Phys. Rev. B: Condens. Matter Mater. Phys.*, 2009, **80**, 155445.
117 K. Nakada, M. Fujita, K. Wakabayashi and K. Kusakabe, *Czech. J. Phys.*, 1996, **46**, 2429–2430.
118 M. Fujita, K. Wakabayashi, K. Nakada and K. Kusakabe, *J. Phys. Soc. Jpn.*, 1996, **65**, 1920–1923.
119 P. Koskinen, S. Malola and H. Häkkinen, *Phys. Rev. Lett.*, 2008, **101**, 115502.
120 K. A. Ritter and J. W. Lyding, *Nat. Mater.*, 2009, **8**, 235–242.

121 X. T. Jia, M. Hofmann, V. Meunier, B. G. Sumpter, J. Campos-Delgado, J. M. Romo-Herrera, H. B. Son, Y. P. Hsieh, A. Reina, J. Kong, M. Terrones and M. S. Dresselhaus, *Science*, 2009, **323**, 1701–1705.
122 J. S. Qi, J. Y. Huang, J. Feng, D. N. Shi and J. Li, *ACS Nano*, 2011, **5**, 3475–3482.
123 Z. Liu, K. Suenaga, P. J. F. Harris and S. Iijima, *Phys. Rev. Lett.*, 2009, **102**, 015501.
124 L. Qi, J. Y. Huang, J. Feng and J. Li, *Carbon*, 2010, **48**, 2354–2360.
125 G. F. Schneider, S. W. Kowalczyk, V. E. Calado, G. Pandraud, H. W. Zandbergen, L. M. K. Vandersypen and C. Dekker, *Nano Lett.*, 2010, **10**, 3163–3167.
126 C. A. Merchant, K. Healy, M. Wanunu, V. Ray, N. Peterman, J. Bartel, M. D. Fischbein, K. Venta, Z. T. Luo, A. T. C. Johnson and M. Drndic, *Nano Lett.*, 2010, **10**, 2915–2921.
127 S. Garaj, W. Hubbard, A. Reina, J. Kong, D. Branton and J. A. Golovchenko, *Nature*, 2010, **467**, 190–193.
128 S. K. Min, W. Y. Kim, Y. Cho and K. S. Kim, *Nat. Nanotechnol.*, 2011, **6**, 162–165.
129 M. Zwolak and M. Di Ventra, *Rev. Mod. Phys.*, 2008, **80**, 141–165.
130 J. Feng, L. Qi, J. Y. Huang and J. Li, *Phys. Rev. B: Condens. Matter Mater. Phys.*, 2009, **80**, 165407.
131 T. Dumitrica, C. M. Landis and B. I. Yakobson, *Chem. Phys. Lett.*, 2002, **360**, 182–188.
132 R. B. Weisman and S. M. Bachilo, *Nano Lett.*, 2003, **3**, 1235–1238.
133 J. C. Charlier, X. Blase and S. Roche, *Rev. Mod. Phys.*, 2007, **79**, 677–732.
134 P. Avouris, *Phys Today*, 2009, **62**, 34–40.
135 J. Liu and M. C. Hersam, *MRS Bull.*, 2010, **35**, 315–321.
136 S. Bae, H. Kim, Y. Lee, X. F. Xu, J. S. Park, Y. Zheng, J. Balakrishnan, T. Lei, H. R. Kim, Y. I. Song, Y. J. Kim, K. S. Kim, B. Ozyilmaz, J. H. Ahn, B. H. Hong and S. Iijima, *Nat. Nanotechnol.*, 2010, **5**, 574–578.
137 K. A. Dill and H. S. Chan, *Nat. Struct. Biol.*, 1997, **4**, 10–19.
138 J. Li, A. Kushima, J. Eapen, X. Lin, X. F. Qian, J. C. Mauro, P. Diep and S. Yip, *PLoS One*, 2011, **6**, e17909.